Computational Materials Science 116 (2016) 44–51

Contents lists available at ScienceDirect

Computational Materials Science

journal homepage: www.elsevier.com/locate/commatsci

Prediction of fracture toughness scatter of composite materials

Yan Li [a,*], Min Zhou [b]

[a] Department of Mechanical and Aerospace Engineering, California State University, Long Beach, CA 90840, USA
[b] The George W. Woodruff School of Mechanical Engineering, School of Materials Science and Engineering, Georgia Institute of Technology, Atlanta, GA 30332-0405, USA

ARTICLE INFO

Article history:
Received 16 July 2015
Received in revised form 26 September 2015
Accepted 28 September 2015
Available online 23 October 2015

Keywords:
Fracture toughness
Microstructure
Weibull distribution
Crack deflection/penetration
Two-point correlation functions

ABSTRACT

Fracture toughness of a composite material is not a deterministic property. This is primarily due to the stochastic nature of its microstructure as well as the activation of different fracture mechanisms during the crack-microstructure interactions. Although Weibull distribution has been widely used to determine the probability of material fracture, its role has been confined to fitting fracture toughness data rather than providing predictive insight of material fracture toughness and the magnitude of scatter. Besides, the Weibull parameters which are obtained through curve fitting carry little physical significance. In this paper, an analytical model is developed to predict fracture toughness in a statistical sense. The Weibull distribution parameters are correlated with the statistical measures of microstructure characteristics and the statistical characterization of the competition between crack deflection and crack penetration at matrix/reinforcement interfaces. Although the quantification is specific to Al_2O_3/TiB_2 composites, the approach and model developed here can be applied to other materials. The established correlations will lead to more reliable material design.

1. Introduction

One of the biggest challenges in material sensitive design is to predict the variation of key material properties such as strength and fracture toughness. It has been proved that the stochastic nature of microstructure is the primary reason for fracture toughness scatter [1–3]. The crack interactions with microstructure can result in different failure mechanisms which ultimately determine the variation of fracture toughness [4,5]. Most of the existing probabilistic models for fracture toughness prediction only consider near crack-tip stress states [6–8]. Information regarding microstructure characteristics and failure mechanisms associated with the crack propagation process is not explicitly included in the model formulations. This is due to the fact that the material heterogeneities at the microstructure level and the interaction of a propagating crack with phases in a microstructure are hard to quantify. Both of them are very random and complicated. Li and Zhou [5] developed a semi-empirical model which allows fracture toughness of Al_2O_3/TiB_2 ceramic composites to be predicted. Although this quantification lends itself to the establishment of relations between the statistical attributes of microstructure, fracture mechanism and the fracture toughness of the material, the material fracture toughness is predicted in an average sense from the CFEM (Cohesive Finite Element Method) simulations in Li and Zhou [2]. Based on the previous work, a modified analytical model is introduced which allows the possible range of fracture toughness values to be predicted as function of microstructure. The Weibull distribution parameters are directly correlated to the two-point correlation functions as well as the quantification of fracture mechanisms. These relations can be used for material reliability design by controlling the fracture toughness scatter through microstructure tailoring.

2. Determination of fracture mechanism during crack-microstructure interactions

For Al_2O_3/TiB_2 ceramic composites, a crack can propagate into Al_2O_3 matrix, TiB_2 reinforcements or along the interface in between. Our attention is primarily focused on the last two scenarios because they are the two competiting fracture mechanisms when a crack interacts with reinforcements. He and Hutchinson [9,10] first proposed an energy based criterion which quantifies the competition between crack deflection and crack penetration when a semi-infinite crack is perpendicular to an infinite planar interface. This criterion is only valid for isotropic bi-material which is symmetrically loaded. Gupta et al. [11,12] extended He and Hutchinson's work to anisotropic materials and developed a stress based criterion to determine the activation of the two competiting fracture mechanisms. Their results were validated through laser spallation experiments. Later on, Martínez and Gupta [13] further

* Corresponding author.

http://dx.doi.org/10.1016/j.commatsci.2015.09.061
0927-0256/

Nomenclature

E_i	Young's modulus (i = 0 or 1)
$\bar{E}$	effective Young's modulus of the composite material
f	volume fraction of reinforcements
$\Phi_m, \Phi_{in}, \Phi_p$	surface energy of matrix cracking, interface debonding and particle cracking
H_m, H_{in}, H_p	fractions of matrix cracking, interface debonding and particle cracking
K_{IC}	fracture toughness
K_0	normalization factor
m	shape parameter
l_m , l_p	crack length associated with interface debonding and particle cracking during single crack-particle interaction
μ_i	shear modulus (i = 0 or 1)
P_{ij}	two-point correlation functions (i = 0 or 1; j = 0 or 1)
P_f	probability of fracture
R	particle radius
U	parameter in determining the competition between crack deflection and crack penetration
U_f	total fracture energy released
ν_i	Poisson's ratio (i = 0 or 1)
$\bar{\nu}$	effective Poisson's ratio of the composite material
ω	crack interaction angle
ω_0	critical crack angle for crack deflection and crack penetration transition
W	total projected crack length

improve the criterion so that both single deflection and double deflection at the interface are considered. This criterion uses quasi-static approximation by assuming crack deflection only occurs under constant loading. Although the above work provides sound theoretical basis for quantifying the competition between crack deflection and crack penetration, these criteria cannot be directly applied to analyze real composite materials. First of all, the reinforcements in real composite materials have finite size. Therefore, the interface cannot be considered as infinite. Besides, it has been proved that the shape of reinforcements also influence the activation of different fracture mechanisms. The shape of reinforcements needs to be quantified and included in the criterion as well.

Based on the previous work, Li and Zhou [5] further extend He and Hutchinson's criterion by including the effects of finite reinforcement size, reinforcement shape and distribution in a two-phase composite material. The criterion is parameterized by

$$U = \frac{1-\beta^2}{a_0(1-\alpha)}\left[|c|^2 + |h|^2 + 2R_e(ch)\right]\bar{\rho}^{a_1}e^{\left(\frac{a_2}{s}\right)} - \frac{\Phi_{in}}{\Phi_p}, \tag{1}$$

to determine the activation of the two competing failure mechanisms. Specifically, interface debonding, which is activated by crack deflection, is predicted when $U > 0$. Otherwise, crack penetration induced reinforcement cracking will be activated instead. In the above relation, $\bar{\rho}$ is the roundness of the reinforcement. s represents the characteristic reinforcement size. Φ_{in} and Φ_p are the surface energies of the interface and reinforcement, respectively. For the Al_2O_3/TiB_2 ceramic composite material considered in this study, Φ_{in} and Φ_p are taken as 78.5 J/m^2 and 102.2 J/m^2, respectively. Although the surface energy of matrix Φ_m is not included in Eq. (1), Φ_m = 21.5 J/m^2 is used for the rest of the study. c and h are coefficients which depend on the crack interaction angle ω as shown in Fig. 1(a). The derivation of c and h as well as other parameters in Eq. (1) are discussed in detail in Li and Zhou [5].

To simplify the problem, we consider circular TiB_2 reinforcement particles in the microstructure. $\bar{\rho}$ and s in Eq. (1) are reduced to 1 and 2R, respectively. Here, R is the particle radius. Fig. 1(a) illustrates the evolution of U as ω varies at R = 30 μm. $0 \leqslant \omega \leqslant \pi/2$ is considered in the formulation. ω_0 is defined as the critical crack angle which signifies the transition from crack penetration to crack deflection. Fig. 1(b) compares the U evolution under different particle sizes. It is noted that $\omega = 0^\circ$ is the most difficult scenario for crack deflection. When the crack gradually deviates from the center plane as ω increases, U increases and create a more favorable condition for crack deflection. It is also observed that the activation of crack deflection is independent of ω when the particle size is sufficiently small. As shown in Fig. 1(b), the calculated U value from Eq. (1) is always above zero when R = 10 μm. As R increases, ω_0 increases accordingly and creates a more demanding requirement for crack deflection. Therefore, large particle is more susceptible to crack penetration. The conclusions predicted above reflect the trends reported in other studies [4,14,15].

It should be noted that the work above only considers single crack-particle interaction. In real crack propagation problems, the crack can have multiple interactions with the particles, which adds extra complexity to the problem. Even for the single crack-particle interaction, different crack paths are activated as ω changes. Since the choice of ω is random, the prediction of upper bound and lower bound of fracture toughness needs to consider all the possible ω values. As shown in Fig. 2, l_{in} and l_p represent the crack length for interface debonding and particle cracking under single crack-particle interaction, respectively. l_{in} and l_p are calculated as

$$\begin{cases} l_{in} = (\pi - 2\omega)R, & \text{if } U > 0, \\ l_p = 2R\cos(\omega), & \text{if } U \leqslant 0. \end{cases} \tag{2}$$

As illustrated in Fig. 2, interface debonding is the only fracture mechanism being activated when R = 10 μm. The maximum crack length is reached at $\omega = 0^\circ$. The same trend is observed when R = 200 μm with particle cracking as the only failure mechanism. The above scenarios represent two extreme cases when the particle size is either very small or very large. When the particle size is in between (for example, when R = 20 μm and 30 μm), the maximum crack length is obtained at ω_0 which is also the point where a fracture mode changes from interface debonding to particle cracking.

As discussed earlier, Eq. (2) only applies to single crack-particle interaction. For multiple crack-particle interactions, it is necessary to statistically parameterize the probability of crack encounter with the particle phase. In this paper, two-point correlation functions are employed for this task. The purpose of using two-point correlation functions is two-fold. First of all, these functions have been proved to be effective for microstructure characterization and generation [2,16,17]. Mathematically, the four two-point correlation functions P_{ij} $(i,j = 0 \text{ or } 1)$ measure the probability of finding a given combination of phases over given distance. Since $P_{00} + P_{01} + P_{10} + P_{11} = 1$, only three of the four two-point correlation functions are independent. For example, P_{11} quantifies the probability to randomly locate both the starting point and ending point in phase 1. It is a function of D which is the distance between the two points. In this study, phase 0 and phase 1 represent matrix and reinforcement, respectively. It can be inferred that both the starting point and ending point will overlap with each other when $D = 0$. P_{11} at $D = 0$ is equivalent to the probability of finding the reinforcement phase over the entire microstructure region, which is actually the volume fraction f as shown in Fig. 3. When $D \to \infty$, the starting point and ending points are not correlated any more.

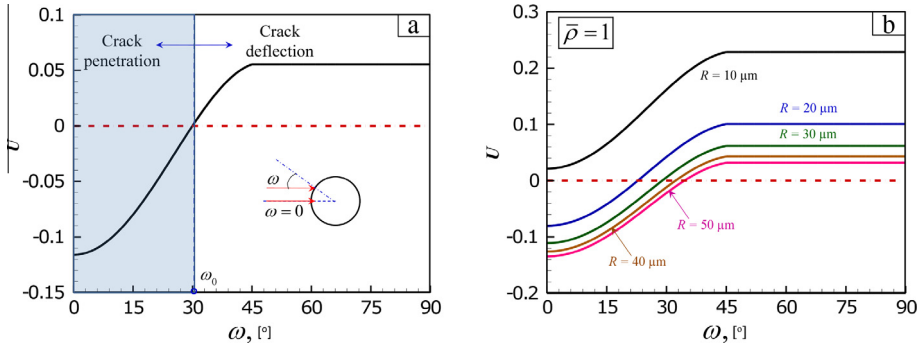

Fig. 1. (a) Criterion U as determination of crack penetration and crack deflection at a matrix/particle interface; (b) U as a function of crack interaction angle ω for different particle sizes.

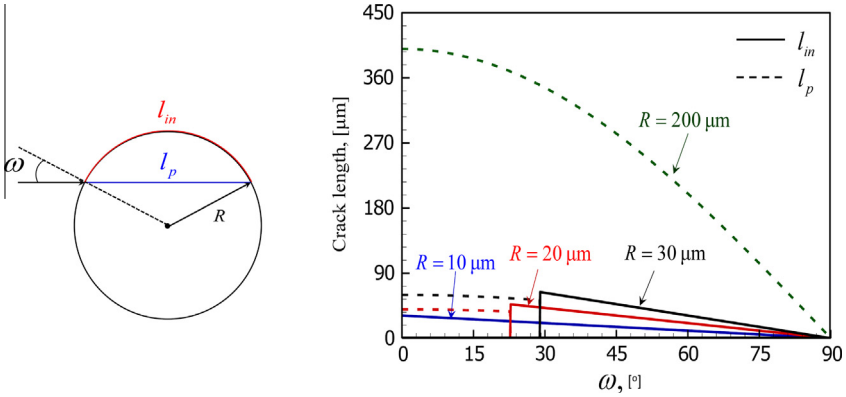

Fig. 2. Schematic illustration of single crack-particle interaction for different particle sizes.

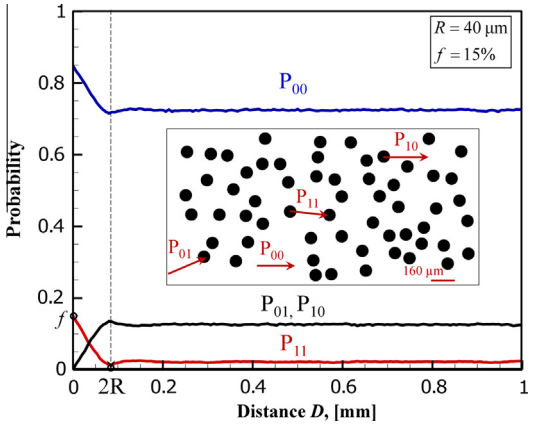

Fig. 3. Two-point correlation functions for two-phase microstructure with $R = 40$ μm and $f = 15\%$.

P_{11} starts to approach f^2, which is the product of locating the starting point and ending point in phase 1 independently. In addition to volume fraction f, the size information of circular reinforcement can be explicitly extracted from two-point correlation functions. The microstructure illustrated in Fig. 3 has randomly distributed uniform circular particles with $R = 40$ μm and volume fraction $f = 15\%$. It can be found that each two-point correlation curve has a peak/dip. The distance $D = 80$ μm which corresponds to the peak/dip is essentially the particle diameter. The above quantifications of two-point correlation functions can be directly used to generate microstructural samples with independently varying geometric characteristics [18].

Two-point correlation functions also provide a means to statistically parameterize the probability of crack interactions with randomly distributed particles in the microstructure. For example, $P_{01}(D)$ quantifies the probability of a crack which is initially in the matrix phase 0 to encounter the reinforcement phase 1 within propagation distance D. As shown in Fig. 3, P_{01} reaches a plateau with the magnitude of $[1 - f^2 - (1-f)^2]/2$ beyond a certain distance D_{cha}. $D_{cha} \approx 100$ μm is the characteristic length of the given microstructure. This indicates that the crack-particle interactions only depend on the volume fraction of the particles if the crack propagation is longer than the characteristic length of the microstructure. Otherwise, the effect of particle size and morphology need to be considered.

Based on the trend and boundary conditions of each two-point correlation curve, a generalized two-point correlation functions can be formulated as

$$\begin{cases} P_{11} = (f - f^2)e^{-(D/2R)} + f^2, \\ P_{00} = \left[(1-f) - (1-f)^2\right]e^{-(D/2R)} + (1-f)^2, \text{ and} \\ P_{01} = P_{10} = (1 - P_{11} - P_{00})/2. \end{cases} \tag{3}$$

These formulations will be used to estimate the crack length associated with each fracture mechanism during the failure process.

As shown in Fig. 4, L_{in}, L_m and L_p represent the crack length associated with interface debonding, matrix cracking and particle cracking, respectively. The total crack length L is a sum of L_{in}, L_m and L_p. W denotes the projection length of the entire crack trajectory. Based on the physical implications of two-point correlations functions, L_{in}, L_p and L_m can be calculated as

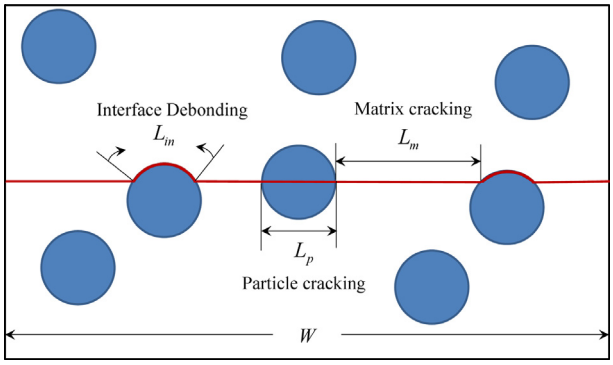

Fig. 4. Schematic illustration of crack lengths associated with different mechanisms in two-phase composite materials.

$$\begin{cases} L_{in}(\omega) = \frac{\int_0^{D_c} P_{01}(D)dx}{D} \cdot N(R,f) \cdot l_{in}, \\ L_p(\omega) = \left(\frac{\int_0^{D_c} P_{01}(D)dx}{D} + \frac{\int_0^{D_c} P_{11}(D)dx}{D} \right) \cdot N(R,f) \cdot l_p, \text{and} \\ L_m(\omega) = L - L_{in}(\omega) - L_p(\omega). \end{cases} \tag{4}$$

Here, N is the total number of particles in the microstructure. N depends on the particle size scale and the volume fraction. For the microstructure configurations with non-overlapping circular particles, N can be calculated as $2f \cdot W^2/\pi R^2$. The distance D_c employed in the integrals is taken as 800 μm. As discussed previously, $D_c = 800$ μm is larger than the characteristic length of the microstructures considered in this study. The crack propagation length is sufficiently long to represent the crack-particle interactions during the failure process. To fully understand the physical meaning of the formulations in Eq. (4), we take L_{in} as an example. The total crack length of interfacial debonding over a distance D_c is the product of (i) the cumulative probability of the crack encountering the particle over D_c, (ii) the total number of particles N in the microstructure, as well as (iii) the crack length of interface debonding under single crack-particle interaction l_{in}. L_p and L_m are formulated by following the same reasoning. In order to make these quantifications dimensionless, L_{in}, L_p and L_m are normalized by the total crack length L as

$$\begin{cases} H_{in} = L_{in}/L, \\ H_p = L_p/L, \text{ and} \\ H_m = L_m/L. \end{cases} \tag{5}$$

H_{in}, H_p and H_m represent the proportions of crack lengths associated with interface debonding, particle cracking and matrix cracking, respectively.

3. Fracture toughness prediction

For brittle materials, the fracture toughness K_{IC} is related to the energy release rate J_{IC} as

$$K_{IC} = \sqrt{J_{IC} \frac{\overline{E}}{1-\bar{\nu}^2}}, \tag{6}$$

where $\overline{E}$ and $\bar{\nu}$ are the effective Young's modulus and effective Poisson's ratio of the heterogeneous material, respectively. $\overline{E}$ and $\bar{\nu}$ are estimated by using the Mori-Tanaka method as

$$\begin{cases} \overline{E} = \frac{9\overline{K}\bar{\mu}}{3\overline{K}+\bar{\mu}} \text{ and} \\ \bar{\nu} = \frac{3\overline{K}-2\bar{\mu}}{6\overline{K}+2\bar{\mu}}, \end{cases} \tag{7}$$

where $\overline{K}$ and $\bar{\mu}$ are effective bulk and shear moduli. $\overline{K}$ and $\bar{\mu}$ are calculated according to

$$\begin{cases} \overline{K} = K_0 + \frac{f(K_1-K_0)(3K_0+4\mu_0)}{3K_1+4\mu_0} \text{and} \\ \bar{\mu} = \mu_0 + \frac{5f\mu_0(\mu_1-\mu_0)(3K_0+4\mu_0)}{3K_0(3\mu_0+2\mu_1)+4\mu_0(2\mu_0+3\mu_1)}. \end{cases} \tag{8}$$

Here, K_r and μ_r represent the bulk and shear modulus, respectively for Al_2O_3 ($r = 0$) and TiB_2 ($r = 1$).

For brittle materials, the total energy released will be completely used to form new crack surfaces. For a crack path involving different types of fracture sites as illustrated in Fig. 4, J_{IC} can be stated as

$$\begin{aligned} J_{IC} &= \frac{\partial U_f}{\partial A} \approx \frac{\left(\Phi_{in}L_{in}+\Phi_m L_m+\Phi_p L_p\right)t}{Wt} \\ &= \frac{L}{W}\left(\Phi_{in}\frac{L_{in}}{L}+\Phi_m\frac{L_m}{L}+\Phi_p\frac{L_p}{L}\right) \\ &= \xi(R,f)\left(\Phi_{in}H_{in}+\Phi_m H_m+\Phi_p H_p\right), \end{aligned} \tag{9}$$

where U_f is the total energy released. $A = Wt$ is the total projected crack surface area with W and t being the crack projection length and specimen thickness, respectively. $\xi = L/W$ is a function which captures the tortuosity of the entire crack path. Based on the microstructure configuration discussed in Section 2, ξ depends on the R and f. H_{in}, H_m and H_p are calculated directly through Eqs. (4) and (5).

It should be noted that the formulations developed in Eq. (9) only applies to quasistatic crack growth for which crack speed approaches zero. It does not account for dynamic fracture induced crack branching, oscillation or micro-cracking. It is assumed that the crack propagation in each single phase always follows a straight path without deflection. For example, the total cracking length L predicted from Eq. (4) is equivalent to the projected length W when $f = 0$ or 1. Based on the assumptions, Eq. (9) underestimates the fracture toughness when dynamic crack propagation is considered. The determination of dynamic fracture toughness requires formulation of dynamic energy release rate as function of crack tip speed and dynamic failure mechanisms involved [19–21]. This part is not considered in this paper but will be included in future publications.

4. Probabilistic fracture toughness analysis

In most of the existing probabilistic models, the fracture toughness data is first obtained from experiment and then fitted by Weibull distribution function [22–24]. A typical two-parameter Weibull distribution function is in the form of

$$P_f = 1 - \exp\left[-\left(\frac{K}{K_0}\right)^m\right]. \tag{10}$$

Here P_f is the probability of fracture. K and K_0 are the fracture toughness K_{IC} measured from experiments and the normalization factor, respectively. m is defined as the shape parameter. The parameters m and K_0 are obtained through a linear regression fit to N data points of K. In order to have a good statistical representation of the stochastic fracture process, $N \geqslant 20$ is preferred.

The problem of the most existing probabilistic models is that they do not allow the scatter of fracture toughness data to be predicted prior to the experimental testing. Without the material sensitivity information, it is hard to determine the number of tests required to obtain a good estimate of probability of material fracture.

Although Weibull parameters in Eq. (10) are fitting parameters which carry little physical significance, their correlations with microstructure characteristics and fracture mechanisms can provide valuable insight to material sensitive design without doing repeated experimental testing. Although experiments can be employed to establish the quantitative relations, these approaches are usually very expensive and time consuming. Besides, experi-

ments are limited to specific material systems. They are not flexible enough to predict the uncertainties of fracture toughness for arbitrary materials, especially materials which are not available now but might be fabricated in the future.

In the following discussions, the K values in Eq. (10) are calculated using the analytical model developed in Sections 2 and 3. Microstructures with non-overlapping circular reinforcements are considered. Fig. 5 compares the probability of fracture P_f for microstructures with systematically varying particle radius ($R = 20$ μm,30 μm and 40 μm) and volume fraction ($f = 10\%$, 15%, 20% and 25%). It is observed that microstructures with smaller radius tend to have higher fracture toughness and lower probability of fracture for all the volume fractions considered. The same trend is observed from the CFEM (Cohesive Finite Element Method) calculations [5] in Fig. 6, where 20 microstructures with same combination of R and f are considered in the analysis. As show in Fig. 5, when f is kept as a constant, the slope of fracture probability curve becomes steeper as R increases, leading to less fracture toughness scatter. The opposite trend is observed when R is fixed while f is increased from 10% to 25%. This indicates that microstructures with fine particles and high volume fractions will have higher-order uncertainties due to the large fracture toughness variation. However, it should be noted that this type of combination also yield higher level fracture toughness values at the same time. This trend has been reported in a few research studies [14,15,25]. From the microstructure design perspective, it is not surprising that shifting up the fracture toughness values will lead to larger scatter band. First of all, composites materials are toughened through crack-particle interactions. Generally speaking, more interactions during the crack propagation process will lead to higher fracture resistance. If a crack does not encounter any reinforcement, the choice of crack path is very limited. The fracture toughness of the composite material is very close to the fracture toughness of matrix material which is considered as the lower bound fracture toughness. Besides, more crack-particle interactions can be created by increasing the volume fraction of particles. As discussed previously, the effective toughening mechanism during crack-particle interaction is crack deflection induced interface debonding. This requires fine particles in addition to high volume fraction. Crack deflection, which contributes to enhancing the level of fracture toughness, also provides the crack with more opportunities in choosing the path. It can be inferred from Fig. 2 that the choice of different arc length leads to larger fracture toughness scatter. The scatter is intensified when more crack-particle interactions are included. This explains why microstructure configurations which lead to higher level of fracture toughness also have larger fracture toughness scatter.

It is also noted that the fracture toughness values predicted from Eqs. (6) and (9) is larger than the values predicted from CFEM results. In Fig. 5, the range of K_{IC} values predicted from the analytical model is approximately from 2.7 MPa$\sqrt{\text{m}}$ to 8.4 MPa$\sqrt{\text{m}}$. In contrast, the range of K_{IC} values predicted from CFEM calculations only spans from 2.7 MPa$\sqrt{\text{m}}$ to 4.7 MPa$\sqrt{\text{m}}$ as shown in Fig. 6. With lower bound K_{IC} predictions being consistent, the analytical model predicts a much higher upper bound value. This is because the two-point correlation functions employed in the analytical model quantify the possibility of crack-particle interactions in the entire microstructure region. However, the crack propagation in CFEM simulations is primarily localized in a small region near the pre-crack plane as illustrated in Fig. 7. The crack does not have the opportunity to interact with particles which are far away from the pre-crack plane. To quantitatively understand how localization of crack propagation influences the level of fracture toughness and the magnitude of scatter, another set of calculations are carried out by considering the interactions of particles within the local region of each microstructure instantiation employed in CFEM calculations. The local region is symmetric with the pre-crack plane with a height of 60 μm as show in Fig. 7.

Fracture toughness scatter is quantified by the shape parameter m. It can be inferred from Eq. (10) that if the magnitude of the scatter is large, then m is small and vice versa. Specially, $m \to \infty$ is expected if there is no scatter. Theoretically, it can be achieved only when $f = 0$ or $f = 1$ as the microstructure is purely matrix phase or reinforcement phase.

Fig. 8 compares m values predicted from the analytical model and CFEM framework. The solid lines and dashed lines represent analytical solutions with the entire microstructure and local microstructure region, respectively. CFEM results are illustrated by dots. Microstructures considered here have volume fraction f ranging from 0% to 30%. Three particle sizes with $R = 20$ μm, $R = 30$ μm and $R = 40$ μm are employed and represented by blue, red and black color, respectively. As demonstrated in Fig. 8, a much higher level of m values are predicted for analytical solutions considering the local microstructure region. This means that there is smaller fracture toughness scatter when the crack only propagates in the localized microstructure region. It makes sense that a lower level of m values are predicted when the entire microstructure region is considered since the interactions of crack with all the particles in the microstructure region are included. From microstructure design prospective, m values predicted by considering the entire microstructure region are very conservative since the crack-particle interaction is usually localized when the reinforcements are well bonded with the matrix. Therefore, analysis with local and entire microstructure region can serve as the upper limit and lower limit of m as represented by dashed and solid lines, respectively. Despite discrepancies in m, both predictions share the same trends. First of all, the increase of volume fraction f leads to decreased m. The larger scatter of fracture toughness is observed due to more intensified crack-particle interactions during crack propagation. The decrease of R can have the same effect as small particles promote interface debonding and create more uncertainties in choosing the crack path. It is noted that the CFEM predictions of m all fall between the upper and lower bound with the similar trends as observed from the analytical predictions. It is also observed that the CFEM predictions are closer to the upper bound m as f increases. When $f = 25\%$, m values predicted from CFEM calculations are very close to the upper bound prediction especially when particle size is small. It can be inferred that the crack-particle interactions in local microstructure region is representative of the entire microstructure region when reinforcements with small size and large volume fractions are considered. As shown in Fig. 8, the discrepancy between the lower bound curves and upper bound curves becomes smaller with increasing f and decreasing R. Once f increases to 100% and R decreases to 0, both the upper and lower bound curves will saturate to $m \to \infty$ as the microstructure becomes pure reinforcement phase. This means m will not continue to decrease as f increases. After f reaches a critical value, the trend reverses. Although the critical f cannot be predicted because the analytical model developed here only considers non-overlapping circular reinforcements, the trends observed from the above analysis are still valid for most engineering cases.

Fig. 9 summarizes the scatter of H_{in} and H_p under different particle size and volume fraction, and compares them with the scatter of fracture toughness m. H_{in}, H_p and m are all predicted from the analytical model considering the local microstructure region. The solid black line in each sub-figure connects the average value of H_{in} or H_p under each volume fraction. It is noted that the scatter of fracture toughness primarily comes of the scatter of H_{in}. The increase in volume fraction f and decrease in particle size R can

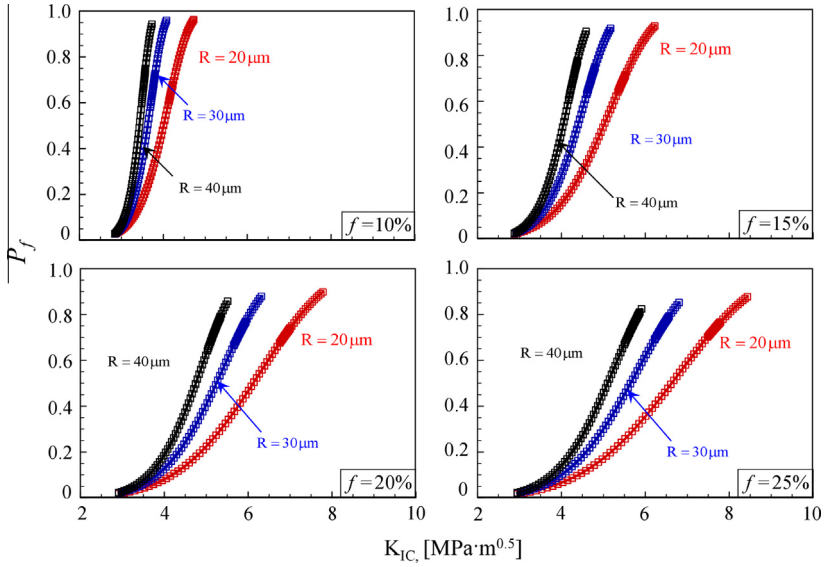

Fig. 5. Fracture probability distribution predicted from analytical model for microstructures with randomly distributed non-overlapping circular particles.

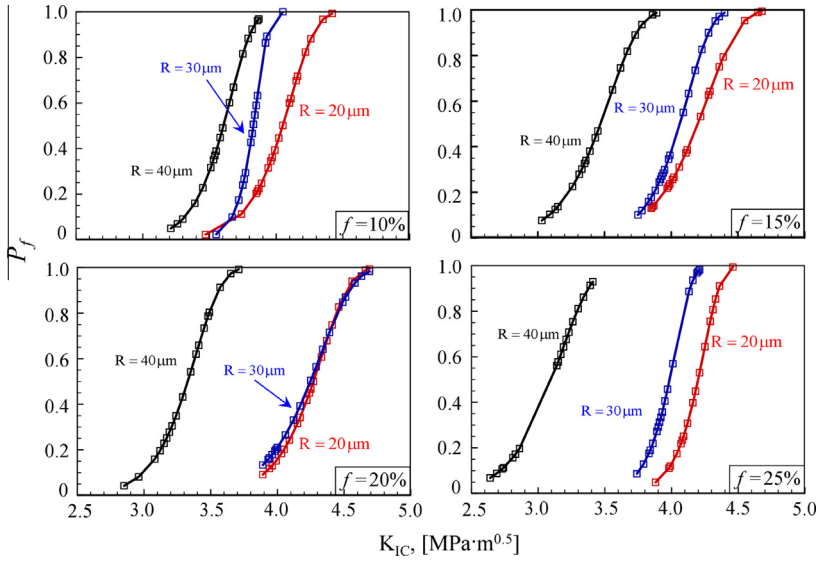

Fig. 6. Fracture probability distribution predicted from CFEM simulations [2] for microstructures with randomly distributed non-overlapping circular particles.

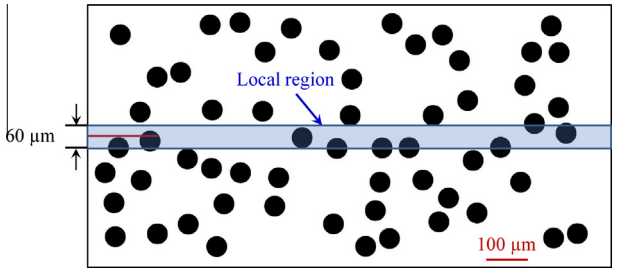

Fig. 7. Scheme of local region for crack propagation observed in CFEM simulations [2].

lead to higher average H_{in} and higher H_{in} as well. Compared with H_{in}, H_p is less sensitive to R and f. The increase in volume fraction f and particle size R has limited effect on the average value of H_p and its scattering.

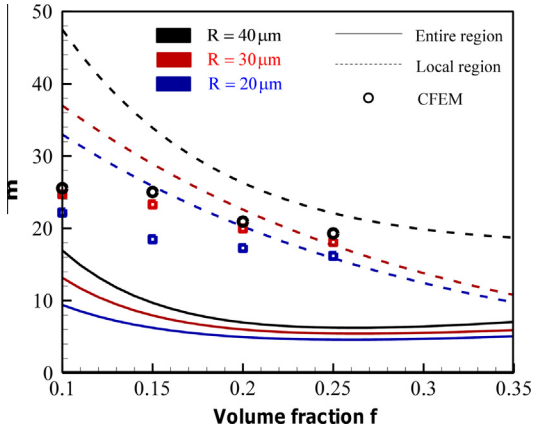

Fig. 8. Effect of microstructure attributes on m predicted from CFEM model and analytical model considering the entire and local microstructure region, respectively.

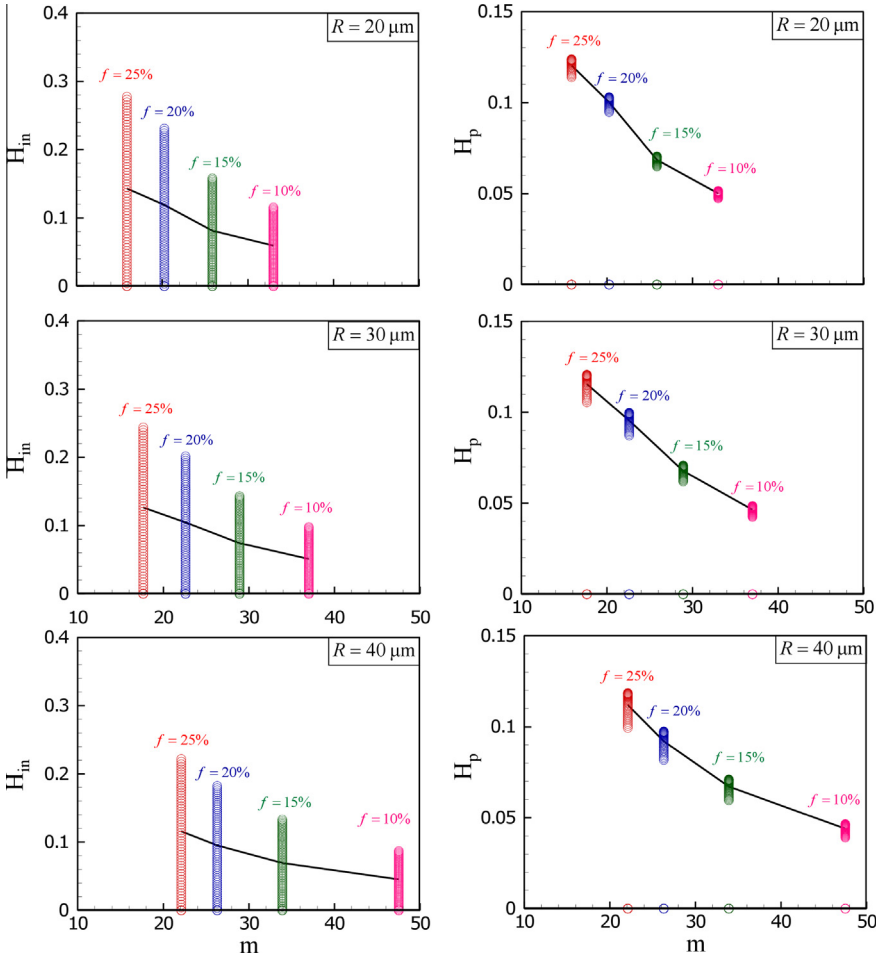

Fig. 9. Effect of proportions of interface debonding H_{in} and particle cracking H_p on m under different values of particle size and volume fraction.

In conclusion, the most effective way to improve the fracture toughness of two-phase composite material is to increase crack tortuosity by promoting interface debonding. This can be achieved by introducing refined second-phase reinforcements with adequate volume fraction. It should be noted that the decrease in reinforcement size and increase in volume fraction also enhance the sensitivity of the material system as larger fracture toughness scatter is observed at the same time. The analytical model developed here provide a way to estimate the upper and lower limit of fracture toughness by considering microstructure attributes and fracture mechanisms involved in the failure process. The prediction of Weibull parameter m as shown in Fig. 8 can be employed as a reference of fracture toughness scatter for material sensitive design of two-phase composite materials.

5. Summary

An analytical model is developed to predict the scatter of fracture toughness of two-phase composite material Al_2O_3/TiB_2 as functions of microstructure attributes and fracture mechanisms involved during the failure process. The Weibull parameter m, which quantifies the scatter of fracture toughness is quantitatively correlated to the geometric attributes of the microstructure as well as the proportion of interface debonding and particle cracking associated with the entire crack path. It is found that increase of interface debonding can result in higher fracture toughness. This fracture mechanism can be promoted by decreasing the reinforcement size and increasing its volume fraction in the dilute situation ($f < 35\%$). Although this type of microstructure tailoring can lead to improved fracture toughness, the material system becomes more sensitive as a larger fracture toughness scatter is observed. The upper and lower bound of fracture toughness scatter predicted here can provide insight to selection of materials and microstructure tailoring without doing repeated testing.

References

[1] K. Strecker, S. Ribeiro, R. Oberacker, M.J. Hoffmann, Int. J. Refract Metal Hard Mater. 22 (2004) 169–175.
[2] Y. Li, M. Zhou, J. Mech. Phys. Solids 61 (Feb 2013) 472–488.
[3] S. Lee, T.H. Kim, D. Kwon, Metall. Mater. Trans. a-Phys. Metall. Mater. Sci. 25 (Oct 1994) 2213–2223.
[4] S. Kumar, W.A. Curtin, Mater. Today 10 (Sep 2007) 34–44.
[5] Y. Li, M. Zhou, J. Mech. Phys. Solids 61 (2013) 489–503. 2//2013.
[6] T.L. Becker, R.M. Cannon, R.O. Ritchie, Eng. Fract. Mech. 69 (Sep 2002) 1521–1555.
[7] B.Z. Margolin, A.G. Gulenko, V.A. Shvetsova, Int. J. Press. Vessels Pip. 75 (Apr 1998) 307–320.
[8] A. Valiente, J. Ruiz, M. Elices, Eng. Fract. Mech. 72 (Mar 2005) 709–728.
[9] M.-Y. He, J.W. Hutchinson, Int. J. Solids. Struct. 25 (1989) 1053–1067.
[10] M.-Y. He, J.W. Hutchinson, J. Appl. Mech. 56 (1989) 270–278.
[11] V. Gupta, A.S. Argon, Z. Suo, J. Appl. Mech. 59 (1992) S79–S87.
[12] V. Gupta, J. Yuan, D. Martinez, J. Am. Ceram. Soc. 76 (1993) 305–315.
[13] D. Martínez, V. Gupta, J. Mech. Physics. Solids. 42 (1994) 1247–1271.
[14] A.G. Evans, J. Am. Ceram. Soc. 73 (Feb 1990) 187–206.
[15] T. Lin, A.G. Evans, R.O. Ritchie, Acta Metall. 34 (Nov 1986) 2205–2216.
[16] S. Torquato, Random Heterogeneous Materials: Microstructure and Macroscopic Properties, Springer, 2002.
[17] A. Tewari, A.M. Gokhale, J.E. Spowart, D.B. Miracle, Acta Mater. 52 (2004) 307–319.
[18] A. Tewari, A.M. Gokhale, J.E. Spowart, D.B. Miracle, Acta Metall. Mater. 52 (2004) 307–319.

[19] K. Ravi-Chandar, W.G. Knauss, Int. J. Fract. 26 (1984) 141–154. 1984/10/01.
[20] A.J. Rosakis, G. Ravichandran, Int. J. Solids Struct. 37 (Jan 2000) 331–348.
[21] L. Roy Xu, Y.Y. Huang, A.J. Rosakis, J. Mech. Phys. Solids 51 (3) (2003) 461–486.
[22] W. Weibull, Ing. Vetenskaps Akad. Handl. 151 (1939) 1–45.
[23] K. Wallin, J. Phys. IV 3 (Nov 1993) 575–584.
[24] K. Wallin, K. Torronen, R. Ahlstrand, B. Timofeev, V. Rybin, V. Nikolaev, et al., Nucl. Eng. Des. 135 (Jun 1992) 239–246.
[25] K.V. Logan, Composite Ceramics, Final Tehnical Report, final technical report, ed: USSTACOM DAAEO7-95-C-R040, 1996.